Achieving good tensile properties in ultrafine grained nickel by spark plasma sintering

Lucía García de La Cruz, Mayerling Martinez, Clément Keller, Eric Hug

Version of Record: https://www.sciencedirect.com/science/article/pii/S0921509319315552
Manuscript_3dbb722eff0dc77799f4a3561bd89583

Achieving good tensile properties in ultrafine grained nickel by Spark Plasma Sintering

Lucía García de la Cruz[a], Mayerling Martinez[a], Clément Keller[b], Eric Hug[a*]

[a]Normandie Univ, UNICAEN, ENSICAEN, CNRS, Laboratoire CRISMAT, 6 Bvd du maréchal Juin 14050 Caen, France

[b]Groupe de Physique des Matériaux,CNRS-UMR6634, Université de Rouen, INSA de Rouen, Avenue de l'Université, 76800 Saint-Etienne du Rouvray, France

* Corresponding author

Abstract

In this work, the tensile properties of ultrafine grain Ni samples processed by spark plasma sintering are investigated. To this aim, a high purity Ni powder was nanostructured by ball milling using different processing conditions, and consolidation of the powder was performed by spark plasma sintering. Milling parameters were varied to produce samples with different microstructures. Each sample was characterised in terms of grain size and grain boundary character distribution to study the influence of milling parameters on the microstructure. Results show that suitable ball milling and subsequent sintering can be employed to obtain specimens with grain sizes in the ultrafine grain range with a high fraction of Σ3 grain boundaries. All samples exhibit a low internal stress state, which is evaluated in terms of grain orientation spread computed from electron backscatter diffraction and dislocation observation by transmission electron microscopy. Uniaxial tensile testing shows an increase in yield strength with grain refinement with a pronounced deviation from the Hall-Petch relation, for samples with grain sizes below 1.2 µm. Heterogeneity in deformation at yielding seems responsible for the deviation due to differences in the strain hardening behaviour between ultrafine grains and conventional coarse grains. All samples display high ductility with values of elongation to fracture above 35 % as well as good toughness. The combination of ball milling with spark plasma sintering is therefore a promising tool to produce ultrafine grain Ni with good mechanical properties.

Keywords: nickel, ball milling, spark plasma sintering, ultrafine grained microstructure, internal stresses, mechanical properties

1. Introduction

Ultrafine grained (UFG) materials are characterised by a microstructure with a grain size typically in the 0.1–1 μm range. The current interest in UFG materials arises from their specific physical properties [1–4], superior mechanical behaviour [5,6], and the attractive combination with other functional properties, such as higher wear resistance [7] or ultrafast diffusion rates [8,9]. The two main techniques to manufacture bulk UFG materials are powder metallurgy and Severe Plastic Deformation (SPD). SPD techniques are more frequently used and studied, however, they are limited by a lack of homogeneity [10], a low ductility [11,12], and the small dimensions of the processed specimens. In addition, the control of the grain size remains difficult with SPD due to the existence of a processing optimum, which leads to the most homogeneous microstructure [6,13,14].

Powder metallurgy can overcome some of the drawbacks of SPD by enabling the synthesis of homogeneous specimens with different microstructures in the UFG range. To this aim, the starting powder consists of either nanopowder or nanostructured powder obtained by ball milling. To preserve the refined microstructure, the precursors are sintered by means of high isostatic pressure (HIP) or spark plasma sintering (SPS). Both techniques apply pressure simultaneously to heating, achieving very fast heating rates and limiting grain growth as reported for various metals and alloys [15–19] including nickel [20]. For this last reference, a low relative density (86 %) and fracture occurring in the elastic regime indicates the presence of oxides, mainly due to the use of nanopowder as starting material. Indeed, sensitivity to oxidation strongly depends on the specific surface area of the powder and thus on the particle size. Such layers of oxides are formed on the surface of the nanoparticles and act as diffusion barriers, avoiding higher densification. Powder nanostructured by ball milling displays a particle size of the order of micrometres being much less susceptible to oxidation.

Varying the ball milling parameters also leads to powders with diverse characteristics, such as morphology, size, and microstructure *i.e.* crystallite size, microstrain and texture [21–23]. The effect of some of these parameters on the resulting powder can be found for several metals and alloys: Al [24–27], Cu [28], TiFe [29] or 316L [30,31]. Research activities concerning Ni have focused on a single parameter, milling time [32,33], or on the properties

of powders after ball milling: oxidative behaviour [34], deformation evolution [35], and solid-state transformations [36]. Nevertheless, to our knowledge, the coupled effects of ball milling and SPS on the microstructure and tensile properties of bulk samples with grain sizes in the UFG regime have not been deeply investigated. This characterisation is of prime importance to ensure the development of powder metallurgy as a valuable tool for the elaboration of UFG metals and alloys.

In the present work, UFG Ni samples with variable grain size were processed by SPS. The obtained microstructure and the initial internal stress level were investigated by means of electron backscatter diffraction (EBSD) and transmission electron microscopy (TEM). Afterwards, uniaxial tensile testing was performed in selected samples to evaluate their mechanical properties. The synthesis parameters were selected to produce samples with different grain sizes in the fine grained (FG)/UFG range, which can involve changes in deformation mechanisms [37–39]. Ductility was investigated as the major drawback in UFG metals, as well as the impact of the refined microstructure in strength (Hall-Petch relation).

2. Experimental procedures

2.1. Ball milling process and characterization of the powder

Nanostructured powders were prepared by high-energy ball milling from a high purity commercial nickel powder provided by Good Fellow©. The powder has a certified purity of 99.8 %, the main impurities being: Fe 100 ppm, C 200 - 600 ppm, O 1000 ppm and S 10 ppm.. Ball milling (BM) was performed in a Fritsh planetary pulverisette 7 using WC vials (80 mL) and grinding balls (5 mm in diameter). Ball-to-powder ratio was fixed to 10:1. In order to modify the characteristics of powders and study their impact on the microstructure of samples after consolidation by SPS, rotation speed and milling time were varied. Time and rotation speed ranges were chosen to limit processing time and probability of contamination from the milling media. Anhydrous methanol was chosen as process control agent (PCA) for its low reaction with Ni powders [40,41] and its low boiling point, making elimination easier. The amount of methanol ranged from 16.7%wt.% to 66.7 wt.% [30], and showed little impact on the corresponding microstructures. Vials were prepared and closed in a glove box with a high purity argon atmosphere in order to avoid oxidation of the powders. The milling time was divided in cycles of 5 min followed by a 1 min pause to reduce overheating which can

enhance powder reactivity. Rotation direction was systematically reversed between cycles to make the process more effective and homogeneous.

Morphology and particle size of the as-received and ball milled powders were analysed by Scanning Electron Microscopy (SEM) using a Zeiss Supra 55. X-ray diffraction (XRD) measurements with a Panalytical X'Pert diffractometer using Cu Kα radiation (λ = 0.1541 nm) were employed to examine the presence of diffraction peaks corresponding to oxides.

2.2. Spark Plasma Sintering

Consolidation of the powders was performed by SPS with a FCT System GmbH, HD25 SPS apparatus. Graphite dies, punches and foils were employed in the synthesis. To limit grain growth, the sintering temperature was set to 1023 K, with a heating rate of 100 K/min by continuous current. Sintering was performed under a medium dynamic vacuum (~0.5 mbar). A thermocouple placed inside a hole in the die a few millimetres from the powder was used to monitor the temperature. A uniaxial force was applied throughout the sintering process. The maximum pressure was set to 75 MPa and a dwell time of 10 min was employed. For microstructural characterisation, disc-like specimens with a diameter of 20 mm and 2 mm in thickness were produced. In addition, 50 mm diameter samples, with a thickness of 6 mm were sintered with the same temperature and pressure cycles to produce tensile testing specimens for uniaxial tensile testing. The homogeneity of the samples was verified by hardness cartographies of the surfaces as performed previously for ceramic materials [42]. An additional sample with a grain size in the coarse-grained range was produced from the as received powder using the sintering conditions employed for the synthesis of UFG samples, with the exception of temperature (1273 K). The density of the bulk samples was determined using an immersion densitometry method (mass accuracy 1 mg).

2.3. Microstructure analysis and mechanical properties

The microstructure of the sintered samples was investigated by means of EBSD. For the sake of accuracy, at least 1000 grains were covered for each sample with a step size ensuring more than 4 points per grain along a given direction. For an optimal surface condition, samples were first mechanically polished with SiC paper and afterwards electropolished using a solution of perchloric acid, 2-butoxyethanol and ethanol at a voltage of 24 V. The TSL OIM® analysis software was used to estimate average grain size, grain boundary character distribution (GBCD), grain orientation spread (GOS), and to study the

crystallographic microtexture of the sintered specimens from their pole figures. Brandon's criterion [43] was used for coincidence site lattice (CSL) fraction determinations, which were calculated on a number basis. The misorientation for determining low angle grain boundaries (LAGBs), was defined as 2°-15° [44]. Basic clean-up was performed before each analysis to eliminate artefacts. In addition, TEM observations were performed on a JEOL 2010 at an operating voltage of 200 kV. The observation of dislocation structures by TEM gave complementary indications to the overall GOS analysis related to the initial internal stress of the samples. Specimens were prepared from 3 mm discs mechanically polished down to approximately 100 µm and then electropolished using a solution of 17 % perchloric acid in ethanol by the twin jet method in a Tenupol 5.

The influence of grain size on the mechanical properties was studied using uniaxial tensile testing up to fracture. From the 50 mm discs, dog-bone tensile samples with a gauge length of 11 mm and a thickness of 1 mm were extracted by electrical discharge machining to avoid sample damage. To remove the roughness induced by the machining, the surface of the specimens were carefully polished with a diamond suspension of 6 µm. Uniaxial tensile testing was carried out at room temperature using a Zwick device with a load cell of 50 kN maximum capacity. Strain rate was fixed to 10^{-3} s^{-1}, and deformation was recorded by measuring displacement fields using digital image correlation (DIC) with the ARAMIS® software. The results reported for each sample correspond to the average of three measurements.

3. Results

3.1 Synthesis and microstructural characterization of SPS processed samples

In addition to grain size, other microstructural features have a major impact on tensile properties, leading to contradictions found in scientific literature concerning the intrinsic characteristics of UFG materials. For instance, Σ3 grain boundaries have been characterised as strong barriers for dislocation motion inducing, in turn, a larger strengthening than random boundaries [45–47]. In this study, BM parameters have been modified to produce microstructures with different grain sizes and GBCD, which are investigated by EBSD.

For the synthesis of the samples, two types of powders were considered, the as-received commercial powder and powders obtained by BM. The as-received powder is

characterised by polycrystalline particles of spherical/cubic "spiky-dendritic" aspect (**Fig.** 1 (a)). It displays an average particle size of 3.5 µm ± 1.5 µm and a narrow particle distribution. Ball milling powders are characterised by highly deformed particles of flattened morphology (**Fig.** 1 (b)). The BM powder evolves at higher milling speed and after longer milling times to a more homogeneous powder with bigger particles as reported in a previous work [48]. The powder displayed in **Fig.** 1 (b) prepared by milling for 3h at 350 rpm, displays an average particle size of 60 ± 22 µm and an approximate thickness of 1 µm.

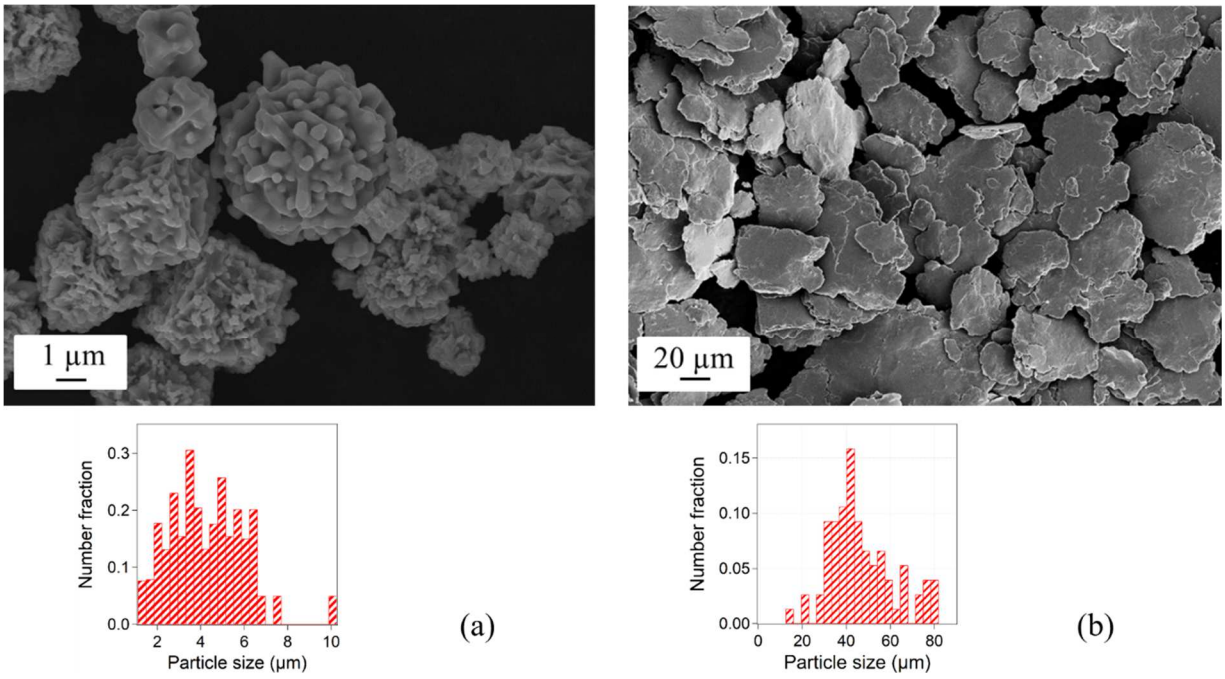

Fig. 1 – SEM image of the as-received powder (a) and BM powder (350 rpm, 3 h) (b), and corresponding particle distribution.

XRD was used to investigate the presence of contamination species such as oxides as well as for texture examination. Diffractograms exclusively displayed peaks that correspond to the face centred cubic (FCC) phase of nickel, irrespective of the conditions of elaboration (**Fig.** 2). No contamination peaks were observed for any powder, or in their corresponding sintered states. Preferred crystallographic orientation in powders was examined from the intensity ratio, I_{200}/I_{111}. This ratio varied between 0.37 and 0.5 depending on the milling conditions, which is close to the value of random orientation I_{200}/I_{111} = 0.42 as determined

from the standard diffractogram for Ni [49]. No marked crystallographic texture was thus observed independently of the elaboration conditions.

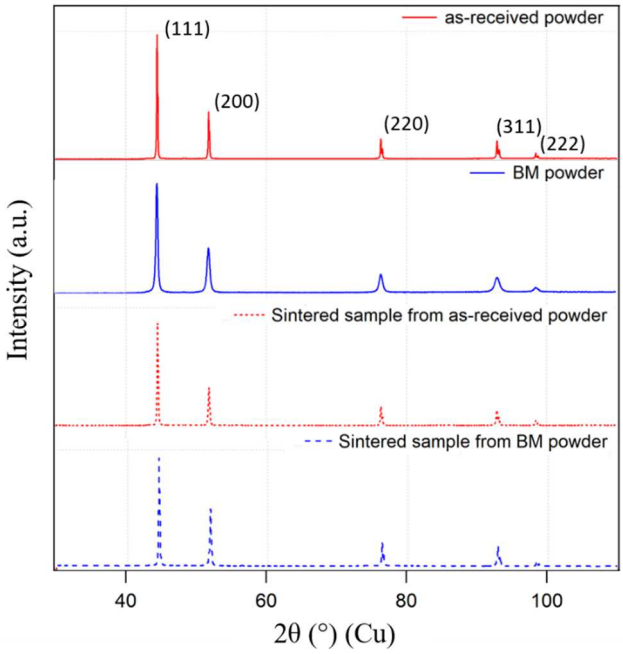

Fig. 2 – XRD diffractograms of the as-received and the BM powder (350 rpm, 3 h) (solid lines), and results of the corresponding sintered specimens (dashed lines).

After sintering, bulk samples with relative densities between 96 % and 99 % were obtained, in agreement with literature [50]. The microstructures were investigated in terms of grain size and GBCD, highlighting Σ3 grain boundaries and LAGBs. The sample sintered from the as-received powder (S-PC) (**Fig.** 3 (a)) exhibits an average grain size of 3.4 µm in agreement with previous values reported for Ni sintered under similar conditions [51,52]. The grain size of the samples processed from BM powder (**Fig.** 3 (b)-(c)) correlates to the milling condition. Thus, an average grain size of 1.43 µm is obtained sintering a powder milled at 200 rpm for 3 hours (**Fig.** 3 (b)) and of 0.79 µm for the same milling time but higher milling speed, 350 rpm (**Fig.** 3 (c)).

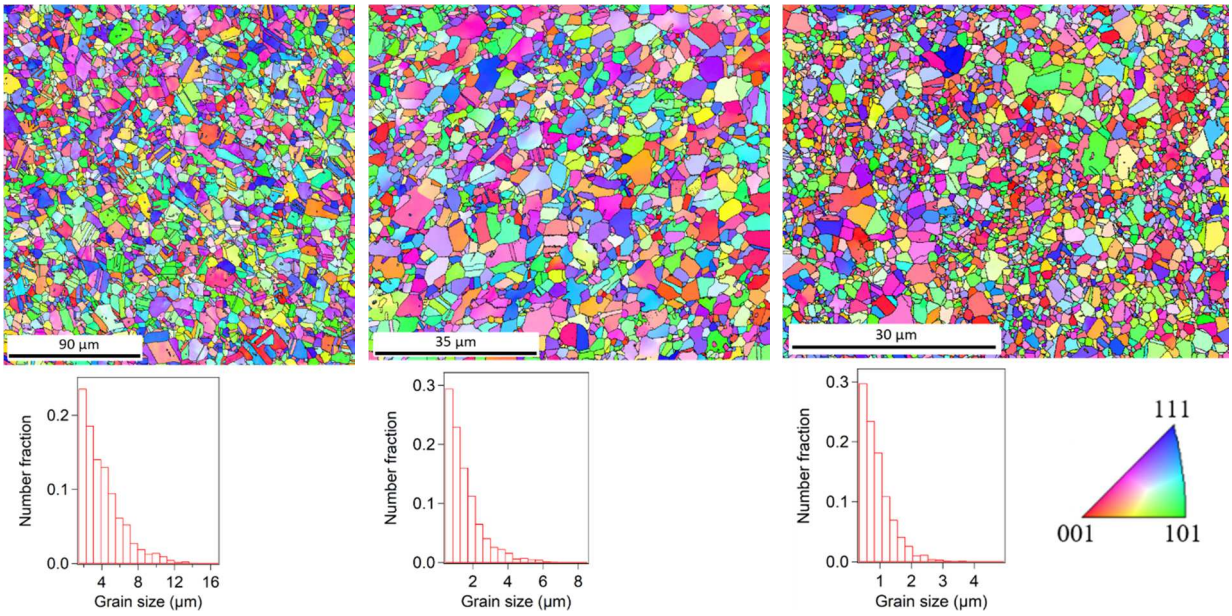

Fig. 3 – EBSD inverse pole figure (IPF) and corresponding grain size distribution for SPS samples with different grain sizes: d = 3.4 µm ± 2.4 (2) µm (S-PC) (a), d = 1.43 µm ± 1.01 (5) µm, prepared from milled powder (3 hours at 200 rpm) (b) and d = 0.79 µm ± 0.47 (6) µm, prepared from milled powder (3 hours at 350 rpm) (c). IPF reference, normal direction to the surface of the sample.

The influence of the milling parameters on the final grain size is summarised in **Fig.** 4. An exponential decrease in grain size with milling time is shown (dashed red line), suggesting that the steady state is achieved after 12 hours, considering a rotation speed of 200 rpm. Such evolution is also observed in other methods that use high deformation for grain refinement, like equal channel angular pressing, in which the number of passes is the key parameter [53]. A linear decrease in the average grain size is observed for increasing rotation speed (**Fig.** 4 (blue line)). Higher speed triggers more energetic collisions [25,54] which, in turn, accelerates plastic strain reducing grain size faster. For instance, the sample processed from the powder obtained after milling for 3 hours at 350 rpm has an average grain size in the same range as the specimen milled for 12 hours at 200 rpm.

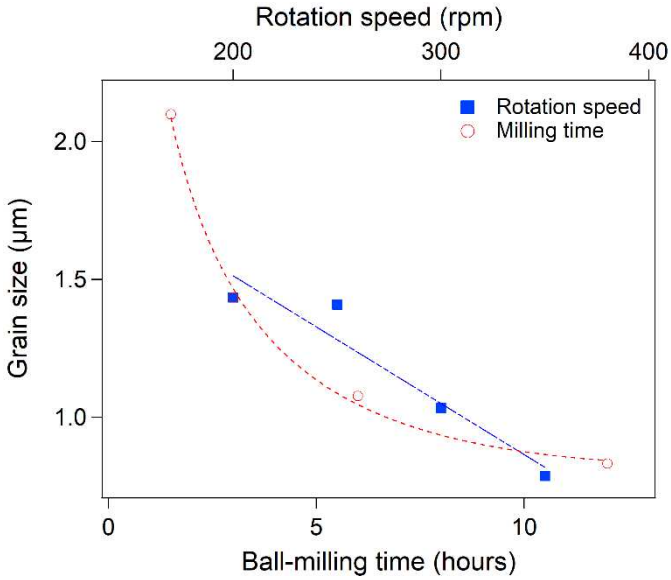

Fig. 4 **–** Effect of milling time (rotation speed of 200 rpm) and rotation speed (milling time of 3 h) on the final grain size of SPS sintered Ni.

The smallest grain size value obtained in the present study is 0.69 ± 0.44 (3) µm. Such sample (labelled S-P0 in the following) was obtained from a powder prepared with a milling time of 10 h (to optimize processing time) and the most severe milling speed, 350 rpm. EBSD analyses of the surface of this sample are displayed in **Fig.** 5 (a). To verify the homogeneity of the microstructure, EBSD was also performed in the cross-section with regard to the SPS applied force direction (**Fig.** 5 (b)). The grain size displayed by this sample in the cross section was 0.65 ± 0.39 (3) µm and differences in GBCD were below 4 % between the two measurements. Pole figures do not reveal any development of crystallographic microtexture. Despite the patterns in the stereographic projection for the <001> pole, showing a slight preference for a cube texture, values of the maximum density pole, 1.8 in surface and 1.7 in cross section, combined with the random patterns in stereographic projections for <011> and <111> poles, confirm that the sample has no strong preferential crystallographic orientation.

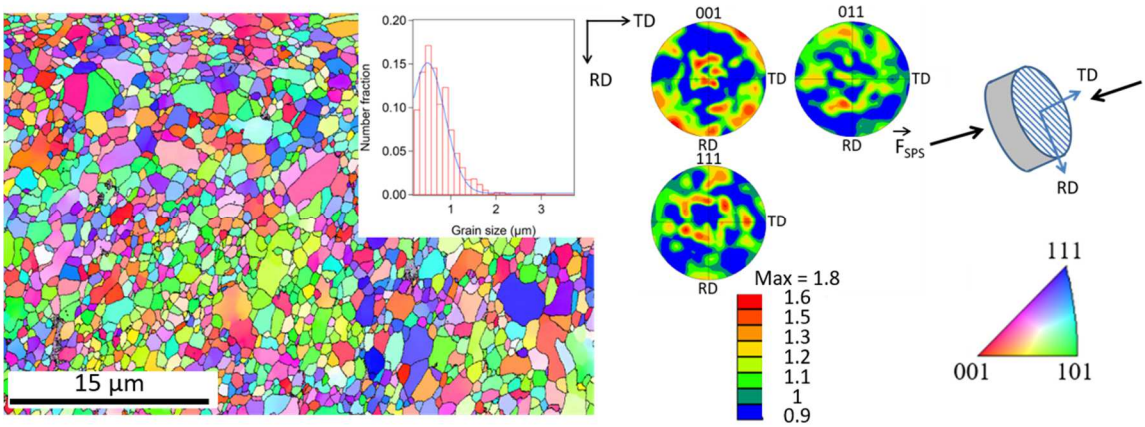

(a)

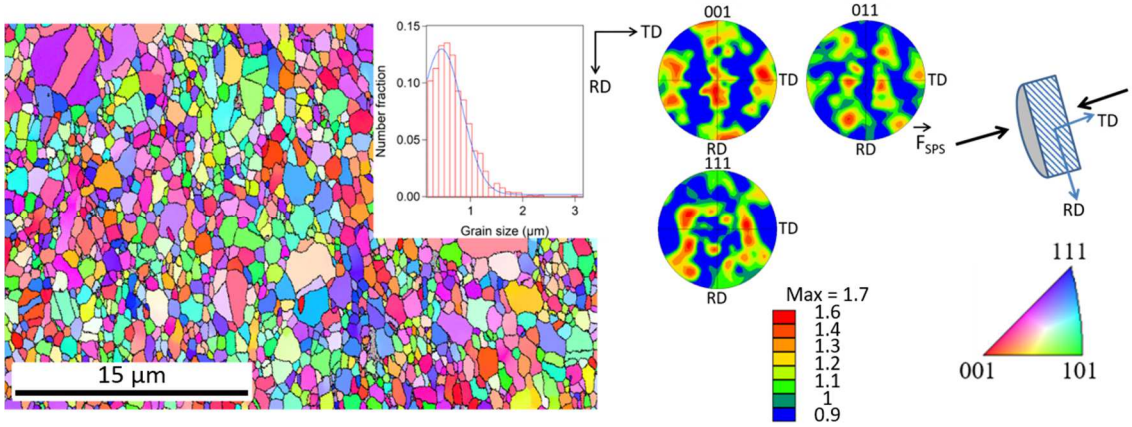

(b)

Fig. 5 **–** EBSD orientation grain map of sample S-P0 (left) with grain size distribution (inset), pole figures (middle) and diagram of the acquisition setting (right) of the sample in surface (a) and cross section (b).

The determination of GBCD for all processed samples revealed a correlation between the fractions of each type of grain boundaries and grain size (**Fig.** 6). The fraction of Σ3 grain boundaries decreases significantly with grain size, especially for values below 1 µm, whereas the fractions of LAGBs and random high angle grain boundaries (HAGBs) increase. The fraction of other CSL (Σ5-Σ29) grain boundaries displays no significant variations. These evolutions can be related to the processing techniques. On the one hand, microstructures obtained by BM are characterised by a high fraction of LAGBs [55,56]. The fast sintering process ensured by SPS hinders the evolution of these boundaries into HAGB, due to the

lower mobility of LAGBs as reported for Cu [58] and Al [59]. Consequently, sample S-P0, prepared with the powder obtained under the most severe milling conditions, displays the highest fraction of LAGBs. Regarding Σ3 boundaries, the high fraction emerges from the intermediate stacking fault energy of nickel [60], which enables the formation of annealing twin boundaries upon sintering. With the exception of the sample with the smallest grain size, in all samples, a high fraction of 75 - 87 % of the Σ3 grain boundaries corresponds to twin boundaries (TB). Deformation and consequent annealing to increase the density of TB has been studied and reported by many authors [61–65]. It explains the elevated fraction of this type of boundaries in the sintered specimens from BM powders, compared to the fractions found in SPD processed UFG nickel (less than 5 %) [66]. In addition, the decrease of the TB density with grain size is in agreement with studies by C.S. Pande *et al.* [67].

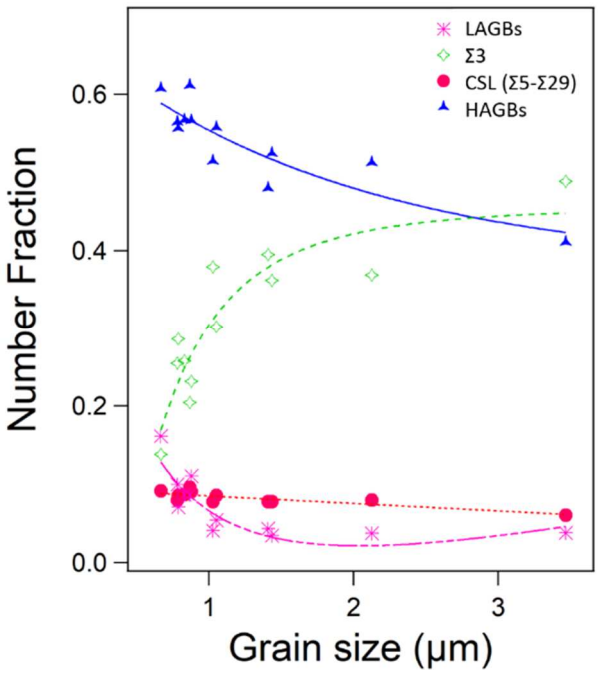

Fig. 6 **–** Evolution with grain size of the fraction of the different types of grain boundaries in UFG sintered Ni.

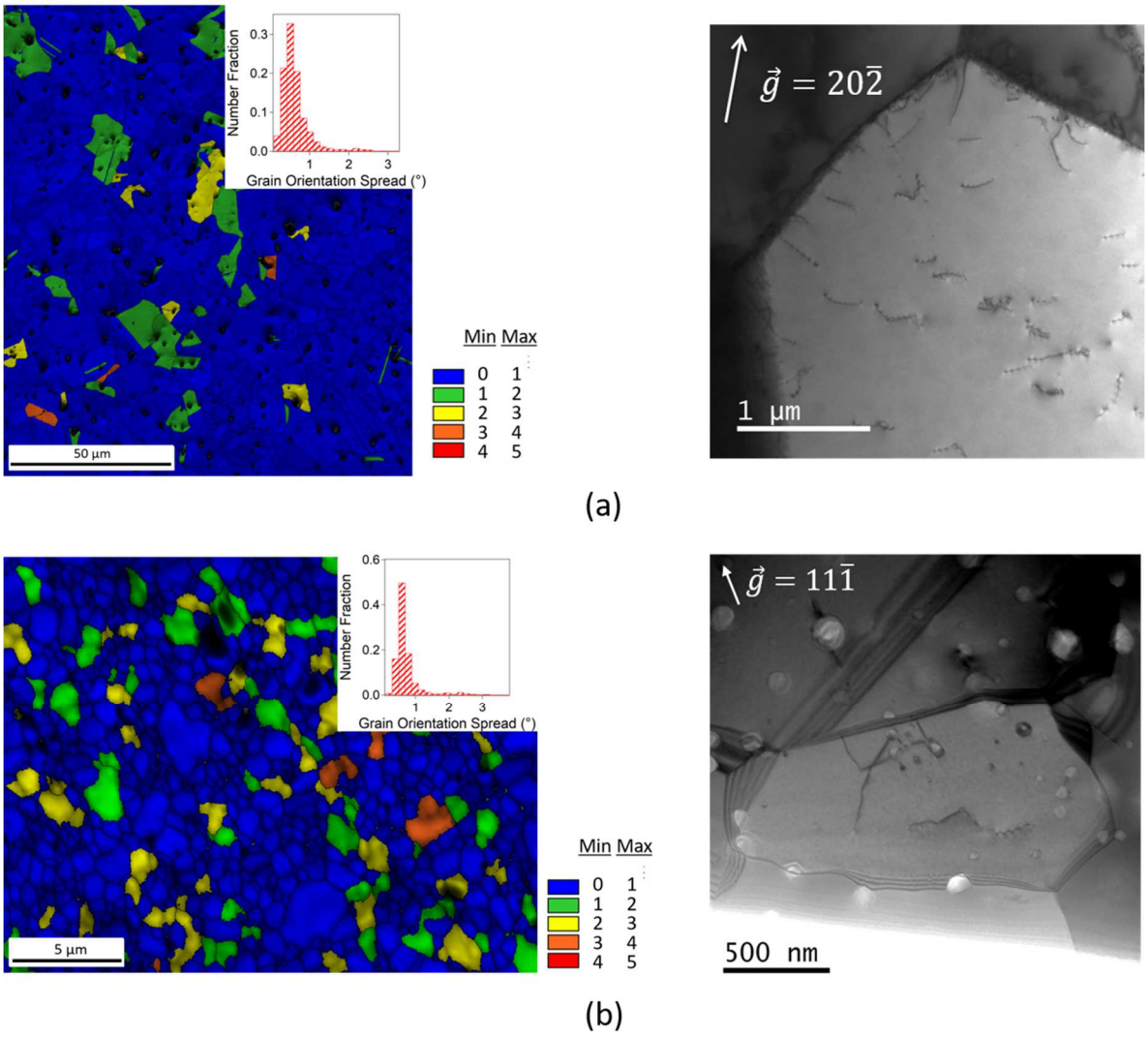

Fig. 7 **–** GOS maps processed from EBSD data obtained for the initial state of samples, d = 3.5 µm (S-PC) (a) and d = 686 nm (S-P0) (b) (left). Bright field TEM images corresponding to the same samples (right).

The initial internal stress state was investigated by grain orientation spread (GOS) obtained from EBSD analyses and the observation of dislocation structures by TEM imaging[1]. GOS represents a statistical measurement of the local weak crystallographic misorientations

[1] Black spots in GOS cartographies correspond to badly indexed zones that match the presence of pores, which become larger by electropolishing. Likewise, pores appear as white spots in TEM images. Porosity structures are displayed at grain boundaries as well as in the bulk of the samples, as confirmed by focused ion beam observations.

existing inside grains and can be related to local internal stress fluctuations. A mean value below 1° corresponds to the stress free internal state displayed by recrystallized samples [68]. **Fig.** 7 (left) displays GOS cartographies for two different grain sizes. In these samples, 88 % (**Fig.** 7 (a)) and 74 % (**Fig.** 7 (b)) of grains display an average misorientation below 1°. GOS histograms (inset to GOS cartographies in **Fig.** 7) verify a statistical distribution centred around 0.5°. More generally, the average GOS determined for all samples is in the range 0.5°-0.8°.

These crystallographic misorientations inside the grains can result from dislocation configurations as evidenced by TEM observations. Sample S-PC (processed from the as-received powder) exhibits mostly defect free grains. Nevertheless, a few grains display some straight dislocation arrangements, as evidenced in the grain displayed in **Fig.** 7 (a) right, which was observed using a diffraction vector $\vec{g} = [20\bar{2}]$, or pile-ups. Sample S-P0, with smaller grain size and observed using a diffraction vector $\vec{g} = [11\bar{1}]$, also displays mainly straight dislocation segments (**Fig.** 7 (b) right) even if small tangles can be scarcely found in some grains. The absence of dislocation cells, together with the existence of straight dislocation segments, few in number, are representative of the weak internal stress level inside UFG specimens, in agreement with GOS results.

3.2 Mechanical properties of UFG Ni processed by SPS

In order to study the influence of grain size in the FG/UFG regime on strength and ductility, five samples were prepared, two from the as-received powder and three from BM powders (**Table** 1). To hinder the influence of GBCD, BM parameters were chosen taking into account the aforementioned results to process samples with different grain sizes and grossly the same fraction of Σ3 grain boundaries. A relative density over 97 % was obtained for all samples.

Table 1 Relative density and synthesis parameters of samples processed for tensile testing.

Sample	ρ_{rel} (%)	Precursor powder	BM time (h)	BM speed (rpm)
1	98.5	BM	10	350
2	99.5	BM	3	350
3	99.3	BM	3	300

4	97.6	As-received	---	---
5	98.7	As-received	---	---

The microstructural characteristics of the five samples are collected in Table 2. Grain size ranges from 0.8 µm to 25 µm. Low GOS is displayed by all samples and a high fraction of Σ3 grain boundaries (above 45 %) can be observed. The density of geometrically necessary dislocations (GNDs) determined from kernel misorientations by EBSD analysis is also collected in **Table** 2. The measurement of GNDs by EBSD is gaining popularity as a useful tool for dislocation quantification to analyse big surfaces of the microstructure, as compared to TEM observations [69,70]. It enables a minimum GND density of about $2x10^{12}$ m^{-2} to be measured with a better sensitivity at low plastic strain levels [71]. GND densities are calculated from the local misorientations inside a grain and using the algorithm already implemented in OIM 8 software. In the present study, a higher density of GNDs is observed in samples prepared from BM powders. ρ_{GND} is also higher for sample 5 than for bulk specimens obtained by casting and careful annealing that display the same grain size (ρ_{GND} = 3-4x10^{12} m^{-2}) [71]. A plastic deformation in tension of 0.08 is needed in cast nickel to obtain the same range of GND density as sample 5, indicating some residual deformation from the applied pressure during sintering. The value of ρ_{GND} obtained for sample 1, the most refined microstructure, is in agreement with results obtained for UFG Ni processed by SPS from nanopowders, ρ_{GND} = 5.1x10^{14} m^{-2} [72].

Table 2 Microstructural features of tensile specimens.

Sample	Grain size (µm)	GOS (°)	LAGB	Σ3	CSL	HAB	ρ_{GND} (m^{-2})
1	0.82 ± 0.67	0.7	0.036	0.495	0.056	0.587	3.5x10^{14}
2	1.11 ± 0.84	0.6	0.04	0.456	0.044	0.54	2.1x10^{14}
3	1.39 ± 1.11	0.7	0.023	0.535	0.057	0.385	2.1x10^{14}
4	4.5 ± 3.3	0.6	0.02	0.526	0.046	0.592	5.1x10^{13}
5	25 ± 17	0.7	0.02	0.616	0.037	0.327	1.4x10^{13}

Corresponding engineering stress-strain curves are provided in **Fig.** 8, showing two distinct tensile behaviours. Samples 3-5 (d > 1.2 µm) exhibit homogeneous plastic deformation. Samples with grain sizes below 1.2 µm display a "Lüders-type" strain at the beginning of the plastic domain, larger in sample 1 than in sample 2, and followed by homogeneous deformation at higher strain.

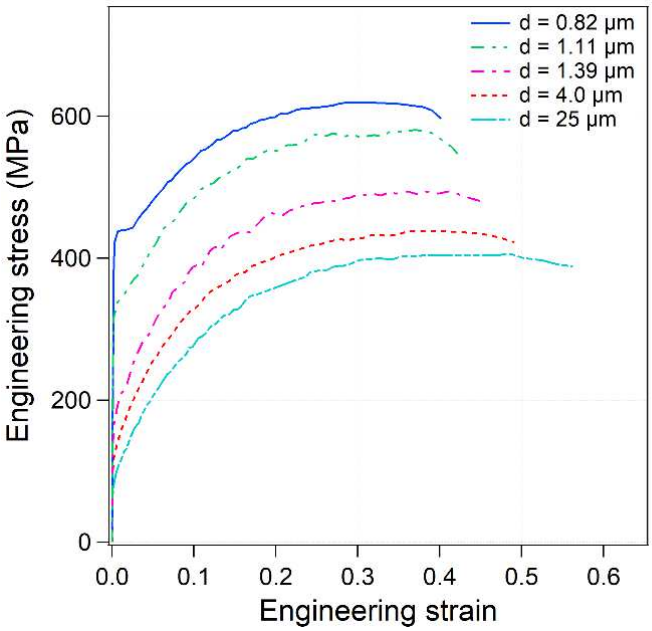

Fig. 8 **–** Engineering tensile curves corresponding to samples processed by SPS with different grain sizes.

Table 3 Tensile characteristics of Ni samples processed by SPS.

Sample	UTS (MPa)	$\sigma_{(0.2\%)}$ (MPa)	ε_f (%)	ε_u (%)	$\sigma_{(0.02\%)} \times \varepsilon_f$
1	625 ± 4	441 ± 7	39 ± 3	30 ± 5	17199 ± 21
2	582 ± 6	325 ± 7	43 ± 1	37 ± 1	13975 ± 7
3	506 ± 8	183 ± 9	46 ± 4	38 ± 4	8418 ± 36
4	443 ± 2	130 ± 2	49 ± 3	41 ± 2	6370 ± 6
5	408 ± 1	87 ± 4	58 ± 3	44 ± 5	5046 ± 12
ECAP + Cold rolling [11]	1050	990	7	---	6930
SPD + heat treatment [11]	890	835	12	---	10020

Table 3 collects the mechanical characteristics in tension of the samples. High yield strength ($\sigma_{(0.2\%)}$) and ultimate tensile strength (UTS) are observed for the UFG samples. The smaller difference between yield strength and the UTS for UFG samples indicates their lower strain-hardening capacity as reported by other authors [12]. Good ductility is displayed by all samples in terms of elongation to fracture (ε_f) and uniform elongation (ε_u). It is noteworthy that for sample 1, ε_f = 39 %, and uniform elongation ε_u = 30 %, which is far above what is reported for UFG Ni processed by SPD [11]. The high fraction of Σ3 grain boundaries in the SPS processed samples may be responsible for the high ductility as reported for Cu [46] and other metals [73].

The product of $\sigma_{(0.2\%)}$ and ε_f is included in Table 3 as an indicator of toughness. For comparison, the value of this product for a SPD processed sample and a sample produced by SPD and subsequent annealing are added. A value three times higher is observed for sample 1 compared to sample 5 and 2.5 times higher than the value obtained for the SPD sample. The specific microstructure obtained by BM and SPS, which combines a reduced grain size with a high fraction of Σ3 grain boundaries, enables the good combination of strength and ductility, especially in specimens with grain sizes in the UFG range.

To investigate the influence of grain size on yield strength, its evolution as a function of $d^{-1/2}$ is plotted (**Fig.** 9). The Hall-Petch (HP) [74] relation provides an expression that relates the two parameters as follows:

$$\sigma_{(0.2)} = \sigma_0 + k_{HP} \cdot \frac{1}{\sqrt{d}} \quad (1)$$

where σ_0 is the friction stress and k_{HP} the HP constant. As a reference, the linear HP fit for nanostructured (NsM)/UFG Ni samples processed by electrodeposition is included in **Fig.** 9 [75]. Such linear fit corresponds to a friction stress of 37 MPa and a HP constant of 175 MPa/μm$^{1/2}$. These values are very close to those previously determined [76] for coarse grained Ni, σ_0 = 14.23 MPa and k_{HP} = 180 MPa/μm$^{1/2}$. A good agreement with the expected values of yield strength is observed for samples 3-5, whereas UFG samples 1-2 strongly deviate from the expected values.

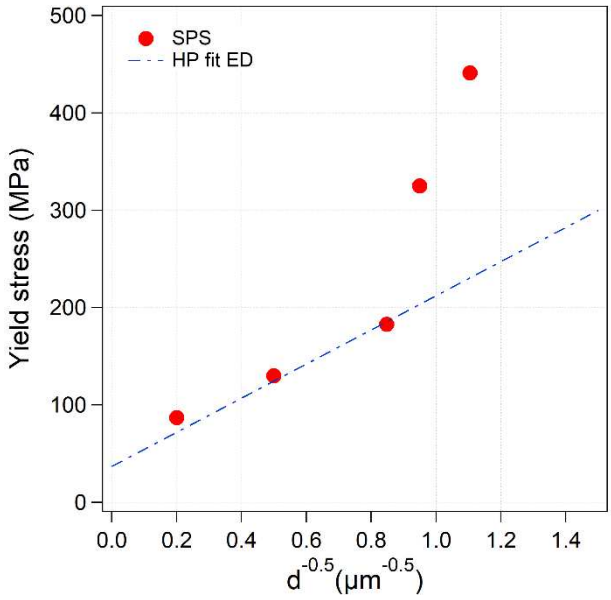

Fig. 9 **–** Grain size dependence of yield strength for Ni samples, in which the dashed line represents a linear fit for UFG Ni processed by electrodeposition [75].

4. Discussion

The results in the previous section show that the synthesis of samples from BM powders and SPS consolidation produces grain sizes in the UFG range with a GBCD characterised by a high fraction of Σ3 grain boundaries and low internal stresses. The sintered samples exhibit good tensile properties despite, especially in the UFG regime, with an improved toughness, a small percentage of porosities.

The grain size dependence on yield strength exhibits a deviation from the expected value from the HP relation in the UFG samples. Such deviation has been reported for UFG Ni processed by other means including SPS sintering of nanopowders [75]. The higher density of dislocations in UFG samples could be at the origin of this deviation as flow stress is related to the total density of dislocations (ρ) following Eq. (2) [77–79]:

$$\sigma = \alpha \mu b M \sqrt{\rho} \qquad (2)$$

where α is an interaction coefficient that depends on the type of interaction between dislocations as well as their configuration, M is the Taylor factor, μ is the shear modulus, and b is the norm of the Burgers vector. The total dislocation density includes GNDs and statistically stored dislocations (SSD). Thus, the higher density of GNDs collected in Table 2 for the UFG samples obtained from BM could account for the extra-strengthening. Assuming,

in first approximation, additive effects of the crystalline defects on the tensile strength [11,75], characterized by Eq. (3), the contribution to strength from GNDs (σ_{GND}) can be evaluated using Eq. (2) considering only the density of GNDs (ρ_{GND}).

$$\sigma = \sigma_{SSD} + \sigma_{GND} + \sigma_{precipitates} + \ldots \quad (3)$$

A new value of strength, can thus be computed by the subtraction of σ_{GND} from the yield strength, $\sigma_{(0.2\%)} - \sigma_{GND}$, to investigate the origin of the HP deviation.

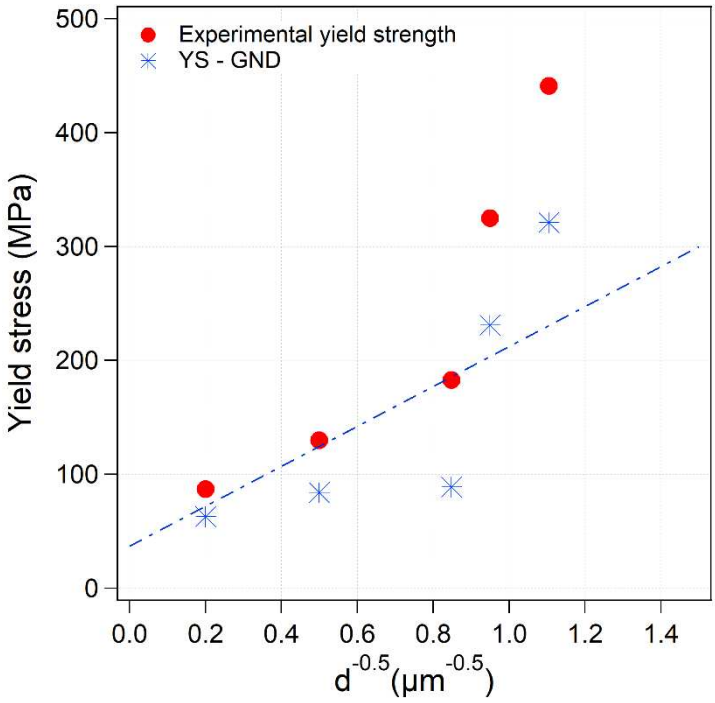

Fig. 10 – Grain size dependence of yield strength (red circles) and computed stress $\sigma_{(0.2\%)} - \sigma_{GND}$ (blue stars).

Fig. 10 illustrates the evolution of $\sigma_{(0.2\%)} - \sigma_{GND}$ as a function of $d^{-1/2}$, for fine and coarse grained samples. In samples 3-5 the effect of grain size in the strength at $\varepsilon = 0.002$ is erased by subtracting the contribution of GNDs as these dislocations are mainly responsible for the grain size strengthening [80]. Nevertheless, an additional strength is always observed in the case of UFG samples, which reveals that another mechanism is linked to this phenomenon.

The origin of such additional stress may be related to the unusual "Lüders-type" strain displayed by the two samples in the UFG regime. This Lüders-type strain has already been

reported for other UFG FCC metals such as Cu [55,81], Al [82] and austenitic stainless steel [83], indicating the occurrence of heterogeneous deformation at the beginning of the plastic domain. In such cases, the average strain measured across the gauge length is not representative of the strain in the deformed zone. Heterogeneity in deformation can be observed in sample 1 from strain cartographies obtained by DIC (**Fig.** 11). In addition, during tensile testing deformation bands in the centre of the gauge length at approximately 45° from the tensile axis were depicted at low strain. C.Y. Yu *et al.* [82] suggest that the origin of such behaviour lies on a microstructure that contains grains with very variable grain sizes that display different deformation behaviours. Yielding is easier in bigger grains, which undergo a pre-yielding microstrain that then percolates to smaller grains, generating homogeneous yielding and deformation. The lower strain hardening reported for small size grains delays the homogenization of deformation, triggering a Lüders-type deformation.

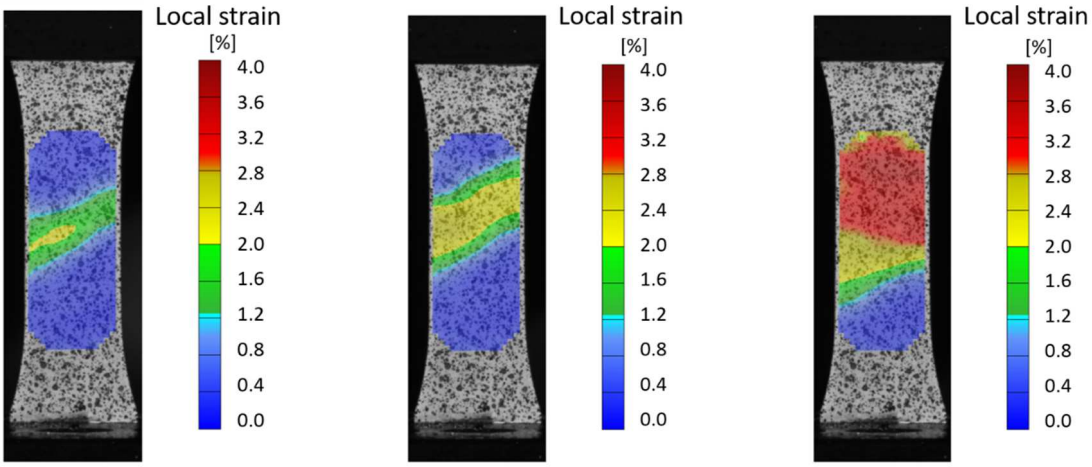

(a) (b) (c)

Fig. 11 **–** Deformation cartographies obtained from DIC at different strain levels: ε = 0.003 (a), ε = 0.009 (b) and ε = 0.02 (c), for sample 1 (d = 0.82 µm).

To eliminate the "heterogeneous yielding factor", C.Y. Yu *et al.* suggest extrapolating the stress at ε = 0.002 using a strain-hardening model capable of describing the deformation behaviour of the investigated samples. In the present case, the true stress-true strain curves can be correctly modelled for coarse-grained samples using the Hollomon model:

$$\sigma = K \cdot \varepsilon^n \quad (4)$$

where σ is the true stress, ε the true strain, K the Hollomon strain-hardening coefficient and n the strain hardening exponent.

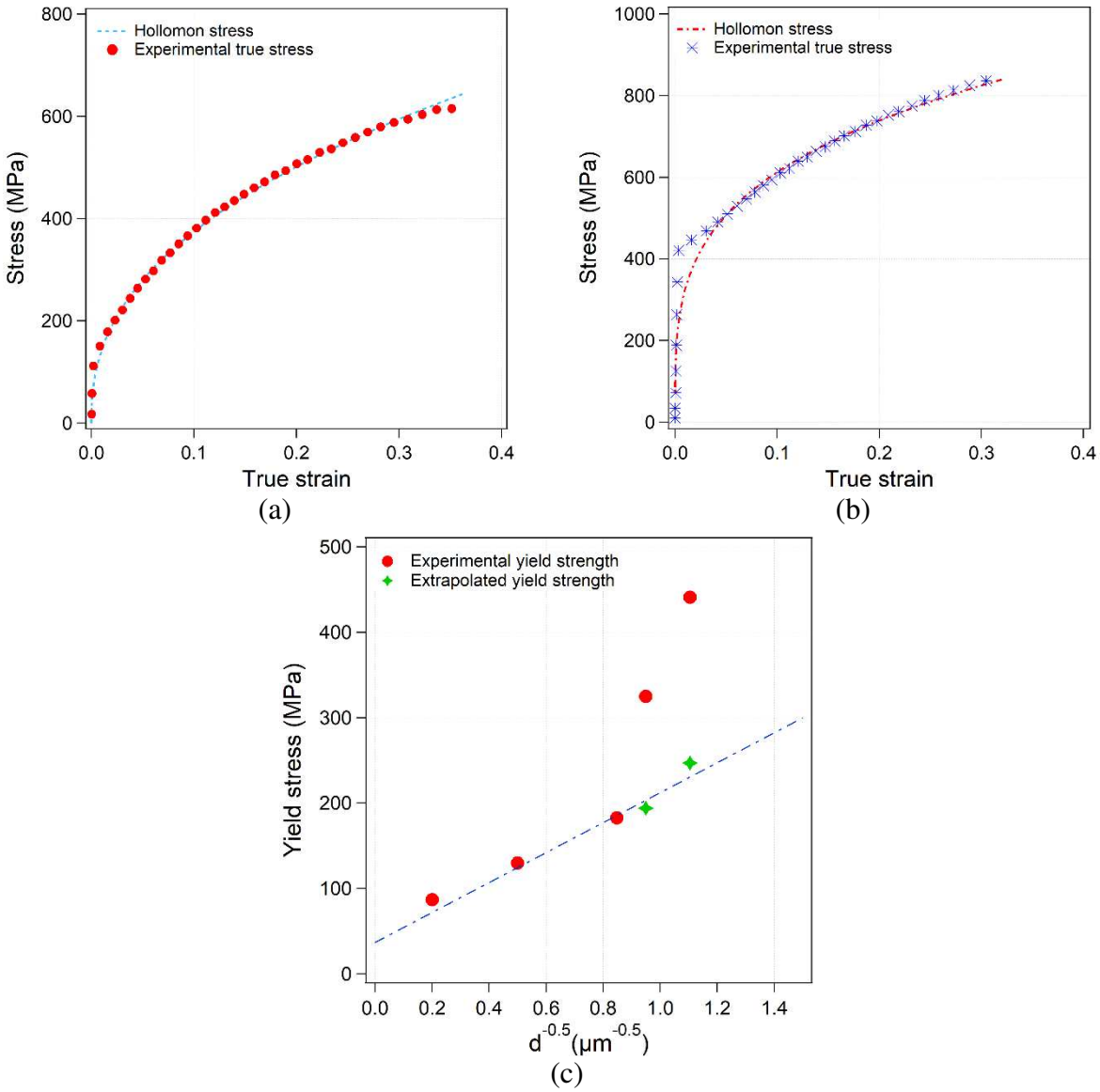

Fig. 12 **–** Computed stress superposed to experimental true stress vs true strain curves for samples 4 (a) and 1 (b). Grain size vs measured yield strength (red circles) and extrapolated yield strength (green stars) for samples 1 and 2 (c).

In **Fig.** 12 (a), the modelled stress and the true stress determined from the experimental data of sample 4 show good agreement. On the other hand, **Fig.** 12 (b) shows that for the UFG

sample 1, the model correctly describes the experimental results only for ε values above 0.05. If the yield strengths for samples 1 and 2 are extrapolated from the modelled curves, the obtained values correspond to the one expected by the HP relation (**Fig.** 12 (c)).

To verify if heterogeneous yielding is the only factor leading to higher stress, true stresses at higher deformation levels were determined and plotted against $d^{-1/2}$ (**Fig.** 13). The HP relation holds for higher levels of deformation [84], thus the persistence of the deviation indicates that other factors should account for the supplementary strengthening. Despite a lower deviation at higher strain, the additional strength that persists through strain hardening could indicate modified plasticity mechanisms specific to the UFG range. In the case of UFG metals obtained by SPD, a deviation from the expected HP relation has also been reported for pure nickel, justified by the presence of dislocation substructures and "non-equilibrium" grain boundaries [85]. Due to the highly deformed nature of BM powders, the existence of such grain boundaries in the UFG samples of this study is possible. Thus, to verify their presence, grain boundary diffusion measurements [86] or high resolution TEM observations [87] of the grain boundaries should be performed.

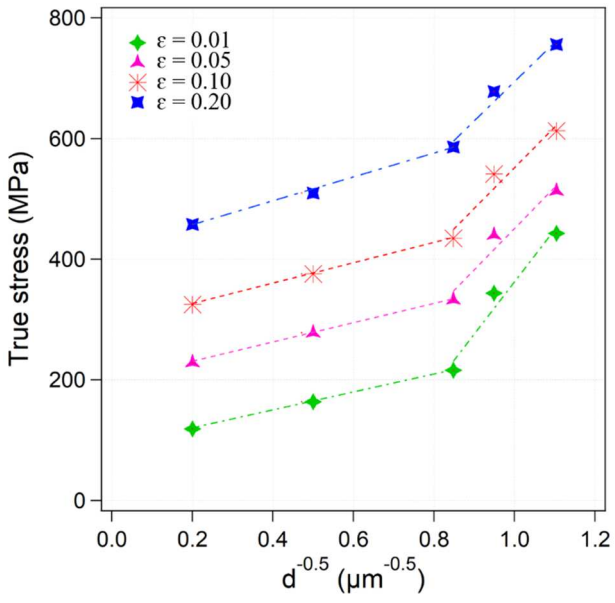

Fig. 13 – Effect of grain size on stress at different deformation levels.

5. Conclusion

UFG Ni samples were successfully produced by nanostructuration of powders via ball milling and subsequent SPS consolidation resulting into highly dense samples with homogeneous microstructures and good tensile properties. The main results obtained in this study can be summarised as follows:

- The synthesis of highly dense samples (relative density > 96 %) with grain sizes in the FG/UFG range can be achieved combining BM and SPS.
- Varying milling conditions enable the synthesis of samples in the FG/UFG range with average grain sizes ranging from 0.6 µm to 3 µm and a GBCD dependent on grain size. A large fraction of Σ3 grain boundaries is depicted, which decreases with grain size.
- GOS analysis and TEM observations illustrate the low internal stress level after SPS processing regardless the final grain size.
- Sintered samples display a good combination of strength and ductility, especially for samples in the UFG regime, with ε_f > 35 % and $\sigma_{0.2\%}$ > 300 MPa.
- A deviation from the HP relation is depicted for samples in the UFG range, which is explained by heterogeneous yielding at yield strength. The persistence of the deviation at higher deformation levels suggests a change in plasticity mechanisms characteristic for UFG samples.

Data Availability Statement

The raw/processed data required to reproduce these findings cannot be shared at this time as the data also forms part of an ongoing study.

References

[1] Y. Huang, T.G. Langdon, Advances in ultrafine-grained materials, Mater. Today. 16 (2013) 85–93.
[2] Y. Estrin, A. Vinogradov, Extreme grain refinement by severe plastic deformation: A wealth of challenging science, Acta Mater. 61 (2013) 782–817.
[3] T.G. Langdon, Twenty-five years of ultrafine-grained materials: Achieving exceptional properties through grain refinement, Acta Mater. 61 (2013) 7035–7059.
[4] R.Z. Valiev, Y. Estrin, Z. Horita, T.G. Langdon, M.J. Zehetbauer, Y. Zhu, Producing Bulk Ultrafine-Grained Materials by Severe Plastic Deformation: Ten Years Later, JOM. 68 (2016) 1216–1226.
[5] R. Valiev, N. Enikeev, M. Murashkin, V. Kazykhanov, X. Sauvage, On the origin of extremely high strength of ultrafine-grained Al alloys produced by severe plastic deformation, Scr. Mater. 63 (2010) 949–952.
[6] M. Kawasaki, R.B. Figueiredo, Y. Huang, T.G. Langdon, Interpretation of hardness evolution in metals processed by high-pressure torsion, J. Mater. Sci. 49 (2014) 6586–6596.

[7] A.P. Zhilyaev, I. Shakhova, A. Belyakov, R. Kaibyshev, T.G. Langdon, Wear resistance and electroconductivity in copper processed by severe plastic deformation, Wear. 305 (2013) 89–99.
[8] P.B. Straumal, M. Wegner, D.V. Shangina, O.A. Kogtenkova, A. Kilmametov, S.V. Divinski, S.V. Dobatkin, G. Wilde, Diffusion of 63Ni in severely deformed ultrafine grained Cu-based alloys, Scr. Mater. 127 (2017) 141–145.
[9] D. Prokoshkina, L. Klinger, A. Moros, G. Wilde, E. Rabkin, S.V. Divinski, Persistence of ultrafast atomic diffusion paths in recrystallizing ultrafine grained Ni, Scr. Mater. 101 (2015) 91–94.
[10] A. Vorhauer, R. Pippan, On the homogeneity of deformation by high pressure torsion, Scr. Mater. 51 (2004) 921–925.
[11] N. Krasilnikov, W. Lojkowski, Z. Pakiela, R. Valiev, Tensile strength and ductility of ultra-fine-grained nickel processed by severe plastic deformation, Mater. Sci. Eng. A. 397 (2005) 330–337.
[12] F. Dalla Torre, P. Spatig, R. Schaublin, M. Victoria, Deformation behaviour and microstructure of nanocrystalline electrodeposited and high pressure torsioned nickel, Acta Mater. 53 (2005) 2337–2349.
[13] A.P. Zhilyaev, G.V. Nurislamova, B.-K. Kim, M.D. Baró, J.A. Szpunar, T.G. Langdon, Experimental parameters influencing grain refinement and microstructural evolution during high-pressure torsion, Acta Mater. 51 (2003) 753–765.
[14] A.P. Zhilyaev, S. Lee, G.V. Nurislamova, R.Z. Valiev, T.G. Langdon, Microhardness and microstructural evolution in pure nickel during high-pressure torsion, Scr. Mater. 44 (2001) 2753–2758.
[15] N. Ouar, M.A. Bousnina, F. Schoenstein, S. Mercone, O. Brinza, S. Farhat, N. Jouini, Spark Plasma Sintering of Co80Ni20 nanopowders synthesized by polyol process and their magnetic and mechanical properties, J. Alloys Compd. 615 (2014) S269–S275.
[16] C. Menapace, G. Cipolloni, M. Hebda, G. Ischia, Spark plasma sintering behaviour of copper powders having different particle sizes and oxygen contents, Powder Technol. 291 (2016) 170–177.
[17] A.J. Song, M.Z. Ma, R.Z. Zhou, L. Wang, W.G. Zhang, C.L. Tan, R.P. Liu, Grain growth and sintering characteristics of Ni–Cu alloy nanopowders consolidated by the spark plasma sintering method, Mater. Sci. Eng. A. 538 (2012) 219–223.
[18] Z. Trzaska, R. Cours, J.-P. Monchoux, Densification of Ni and TiAl by SPS: kinetics and microscopic mechanisms, Metall. Mater. Trans. A. 49 (2018) 4849–4859.
[19] Q.H. Bui, X.T. Pham, Modeling of microstructure effects on the mechanical behavior of ultrafine-grained nickels processed by hot isostatic pressing, Int. J. Mech. Sci. 53 (2011) 812–826.
[20] M.A. Bousnina, A. dakhlaoui Omrani, F. Schoenstein, P. Madec, H. Haddadi, L.S. Smiri, N. Jouini, Spark plasma sintering and hot isostatic pressing of nickel nanopowders elaborated by a modified polyol process and their microstructure, magnetic and mechanical characterization, J. Alloys Compd. 504 (2010) S323–S327.
[21] T. Prasad Yadav, R. Manohar Yadav, D. Pratap Singh, Mechanical Milling: a Top Down Approach for the Synthesis of Nanomaterials and Nanocomposites, Nanosci. Nanotechnol. 2 (2012) 22–48.
[22] C.C. Koch, Synthesis of nanostructured materials by Mechanical Milling: problems and opportunities, NanoStructured Mater. 9 (1997) 13–22.
[23] C. Suryanarayana, Mechanical alloying and milling, Prog. Mater. Sci. 46 (2001) 1–184.
[24] M. Ramezani, T. Neitzert, Mechanical milling of aluminum powder using planetary ball milling process, JAMME. 55 (2012) 790–798.
[25] S.S. Razavi-Tousi, J.A. Szpunar, Effect of ball size on steady state of aluminum powder and efficiency of impacts during milling, Powder Technol. 284 (2015) 149–158.
[26] J.M. Mendoza-Duarte, I. Estrada-Guel, C. Carreño-Gallardo, R. Martínez-Sánchez, Study of Al composites prepared by high-energy ball milling; Effect of processing conditions, J. Alloys Compd. 643 (2015) S172–S177.
[27] A.S. Khan, B. Farrokh, L. Takacs, Effect of grain refinement on mechanical properties of ball-milled bulk aluminum, Mater. Sci. Eng. A. 489 (2008) 77–84.
[28] O. Boytsov, A.I. Ustinov, E. Gaffet, F. Bernard, Correlation between milling parameters and microstructure characteristics of nanocrystalline copper powder prepared via a high energy planetary ball mill, J. Alloys Compd. 432 (2007) 103–110.
[29] R. Neto Mendes Leal, R. Bolsoni Falcão, E.D. Campos Carneiro Dammann, C.J. da Rocha, Mechanical Alloying: An Investigation on the High-Energy Ball Milling of Iron-Titanium Powder Mixtures without Process Control Agents, in: Eur. Congr. Exhib. Powder Metall. Eur. PM Conf. Proc., The European Powder Metallurgy Association, 2010: p. 1.
[30] C. Keller, K. Tabalaiev, G. Marnier, J. Noudem, X. Sauvage, E. Hug, Influence of spark plasma sintering conditions on the sintering and functional properties of an ultra-fine grained 316L stainless steel obtained from ball-milled powder, Mater. Sci. Eng. A. 665 (2016) 125–134.
[31] G. Marnier, C. Keller, J. Noudem, E. Hug, Functional properties of a spark plasma sintered ultrafine-grained 316L steel, Mater. Des. 63 (2014) 633–640.

[32] E. Bonetti, E.G. Campari, L. Pasquini, E. Sampaolesi, G. Scipione, Magnetoelasticity and internal strains in nanocrystalline nickel, NanoStructured Mater. 12 (1999) 817–820.
[33] L. Daroczi, D.L. Beke, G. Posgay, M. Kis-Varga, Magnetic properties of Ball Milled Nanocrystalline Ni and Fe, NanoStructured Mater. 6 (1995) 981–984.
[34] S. Kar, V. Singh, Structural investigations of oxidative behavior on nanocrystalline nickel, J. Alloys Compd. 509 (2011) 3582–3586.
[35] S. Garroni, Deformation conditions for Ni powders undergoing mechanical processing, J. Phys. Chem. Solids. 73 (2012) 770–776.
[36] A.S. Bolokang, M.J. Phasha, Solid-state transformation in ball milled nickel powder, Mater. Lett. 64 (2010) 1894–1897.
[37] E. Hug, P.A. Dubos, C. Keller, Temperature dependence and size effects on strain hardening mechanisms in copper polycrystals, Mater. Sci. Eng. A. 574 (2013) 253–261.
[38] E. Hug, P.A. Dubos, C. Keller, L. Duchêne, A.M. Habraken, Size effects and temperature dependence on strain-hardening mechanisms in some face centered cubic materials, Mech. Mater. 91 (2015) 136–151.
[39] C. Keller, E. Hug, X. Feaugas, Microstructural size effects on mechanical properties of high purity nickel, Int. J. Plast. 27 (2011) 635–654.
[40] A. Arias, Chemical reactions of metal powders with organic and inorganic liquids during ball milling, NASA Tech. Note. D-8015 (1975).
[41] A. Arias, The Role of Chemical Reactions in the Mechanism of Comminution of Ductile Metals into Ultrafine Powders by grinding, NASA Tech. Note. D-4862 (1968).
[42] C. Bourgès, M. Gilmas, P. Lemoine, N.E. Mordvinova, O.I. Lebedev, E. Hug, V. Nassif, B. Malaman, R. Daou, E. Guilmeau, Structural analysis and thermoelectric properties of mechanically alloyed colusites, J. Mater. Chem. C. 4 (2016) 7455–7463.
[43] A.H. King, S. Shekhar, What does it mean to be special? The significance and application of the Brandon criterion, J. Mater. Sci. 41 (2006) 7675–7682.
[44] V. Randle, The coincidence site lattice and the 'sigma enigma,' Mater. Charact. 47 (2001) 411–416.
[45] F. Yuan, X. Wu, Size effect and boundary type on the strengthening of nanoscale domains in pure nickel, Mater. Sci. Eng. A. 648 (2015) 243–251.
[46] L. Lu, S. Yongfeng, X. Chen, L. Qian, K. Lu, Ultrahigh Strength and High Electrical Conductivity in Copper, Science. 304 (2004) 422–426.
[47] L. Lu, R. Schwaiger, Z.W. Shan, M. Dao, K. Lu, S. Suresh, Nano-sized twins induce high rate sensitivity of flow stress in pure copper, Acta Mater. 53 (2005) 2169–2179.
[48] L.G. de la Cruz, B. Flipon, C. Keller, M. Martinez, E. Hug, Nanostructuration of metals via spark plasma sintering using activated powder obtained by ball-milling: Impact on the strain-hardening mechanisms, in: 2017: p. 200002.
[49] R.Z. Valiev, R.S. Mishral, J. Grozal, A.K. Mukherjee, Processing of nanostructured nickel by severe plastic deformation consolidation of ball-milled powder, Scr. Mater. 34 (1996) 1443–1448.
[50] T. Borkar, R. Banerjee, Influence of spark plasma sintering (SPS) processing parameters on microstructure and mechanical properties of nickel, Mater. Sci. Eng. A. 618 (2014) 176–181.
[51] P.P. Bhattacharjee, S.K. Sinha, A. Upadhyaya, Effect of sintering temperature on grain boundary character distribution in pure nickel, Scr. Mater. 56 (2007) 13–16.
[52] G.-D. Dutel, P. Langlois, D. Tingaud, G. Dirras, Room-temperature deformation micro-mechanisms of polycrystalline nickel processed by spark plasma sintering, Mater. Charact. 79 (2013) 76–83.
[53] F. Liu, H. Yuan, J. Yin, J.T. Wang, Influence of stacking fault energy and temperature on microstructures and mechanical properties of fcc pure metals processed by equal-channel angular pressing, Mater. Sci. Eng. A. 662 (2016) 578–587.
[54] G.B. Schaffer, P.G. McCormick, On the kinetics of mechanical alloying, Metall. Trans. A. 23 (1992) 1285–1290.
[55] K.N. Zhu, A. Godfrey, N. Hansen, X.D. Zhang, Microstructure and mechanical strength of near- and sub-micrometre grain size copper prepared by spark plasma sintering, Mater. Des. 117 (2017) 95–103.
[56] C.T. Wang, A.G. Fox, T.G. Langdon, Microstructural evolution in ultrafine-grained titanium processed by high-pressure torsion under different pressures, J. Mater. Sci. 49 (2014) 6558–6564.
[57] D.B. Bober, A. Khalajhedayati, M. Kumar, T.J. Rupert, Grain Boundary Character Distributions in Nanocrystalline Metals Produced by Different Processing Routes, Metall. Mater. Trans. A. 47 (2016) 1389–1403.
[58] N. Liang, Y. Zhao, Y. Li, T. Topping, Y. Zhu, R.Z. Valiev, E.J. Lavernia, Influence of microstructure on thermal stability of ultrafine-grained Cu processed by equal channel angular pressing, J. Mater. Sci. 53 (2018) 13173–13185.
[59] Y. Huang, F.J. Humphreys, Subgrain growth and low angle boundary mobility in aluminium crystals of orientation {110}〈001〉, Acta Mater. 48 (2000) 2017–2030.

[60] N.M. Rosengaard, H.L. Skriver, Calculated stacking-fault energies of elemental metals, Phys. Rev. B. 47 (1993) 12865–12873.
[61] D. Horton, C.B. Thomson, V. Randle, Aspects of twinning and grain growth in high purity and commercially pure nickel, Mater. Sci. Eng. A. 203 (1995) 408–414.
[62] Y. Jin, B. Lin, M. Bernacki, G.S. Rohrer, A.D. Rollett, N. Bozzolo, Annealing twin development during recrystallization and grain growth in pure nickel, Mater. Sci. Eng. A. 597 (2014) 295–303.
[63] S. Mahajan, C.S. Pande, M.A. Imam, B.B. Rath, Formation of annealing twins in fcc crystals, Acta Mater. 45 (1997) 2633–2638.
[64] H. Gleiter, The formation of annealing twins, Acta Metall. 17 (1969) 1421–1428.
[65] V. Randle, P.R. Rios, Y. Hu, Grain growth and twinning in nickel, Scr. Mater. 58 (2008) 130–133.
[66] K.S. Raju, M.G. Krishna, K.A. Padmanabhan, K. Muraleedharan, N.P. Gurao, G. Wilde, Grain size and grain boundary character distribution in ultra-fine grained (ECAP) nickel, Mater. Sci. Eng. A. 491 (2008) 1–7.
[67] C.S. Pande, M.A. Imam, B.B. Rath, Study of annealing twins in FCC metals and alloys, Metall. Trans. A. 21 (1990) 2891–2896.
[68] K. Sitarama Raju, M. Ghanashyam Krishna, K.A. Padmanabhan, V. Subramanya Sarma, N.P. Gurao, G. Wilde, Microstructure evolution and hardness variation during annealing of equal channel angular pressed ultra-fine grained nickel subjected to 12 passes, J. Mater. Sci. 46 (2011) 2662–2671.
[69] C. Fressengeas, B. Beausir, C. Kerisit, A.-L. Helbert, T. Baudin, F. Brisset, M.-H. Mathon, R. Besnard, N. Bozzolo, On the evaluation of dislocation densities in pure tantalum from EBSD orientation data, Matér. Tech. 106 (2018) 1–14.
[70] C. Moussa, M. Bernacki, R. Besnard, N. Bozzolo, Statistical analysis of dislocations and dislocation boundaries from EBSD data, Ultramicroscopy. 179 (2017) 63–72.
[71] O. Muransky, L. Balogh, M. Tran, C.J. Hamelin, J.-S. Park, M.R. Daymond, On the measurement of dislocations and dislocation substructures using EBSD and HRSD techniques, Acta Mater. 175 (2019) 297–313.
[72] J. Gubicza, H.-Q. Bui, F. Fellah, G.F. Dirras, Microstructure and mechanical behavior of ultrafine-grained Ni processed by different powder metallurgy methods, J. Mater. Res. 24 (2009) 217–226.
[73] M.A. Meyers, A. Mishra, D.J. Benson, Mechanical properties of nanocrystalline materials, Prog. Mater. Sci. 51 (2006) 427–556.
[74] E.O. Hall, The deformation and ageing of mild steel: III discussion of results, Proc. Phys. Soc. Sect. B. 64 (1951) 747.
[75] Q.H. Bui, G. Dirras, S. Ramtani, J. Gubicza, On the strengthening behavior of ultrafine-grained nickel processed from nanopowders, Mater. Sci. Eng. A. 527 (2010) 3227–3235.
[76] C. Keller, E. Hug, Hall–Petch behaviour of Ni polycrystals with a few grains per thickness, Mater. Lett. 62 (2008) 1718–1720.
[77] U.F. Kocks, H. Mecking, Physics and phenomenology of strain hardening: the FCC case, Prog. Mater. Sci. 48 (2003) 171–273.
[78] H. Mecking, U.F. Kocks, Kinetics of flow and strain-hardening, Acta Metall. 29 (1981) 1865–1875.
[79] D. Kuhlmann-Wilsdorf, Theory of plastic deformation:-properties of low energy dislocation structures, Mater. Sci. Eng. A. 113 (1989) 1–41.
[80] M.F. Ashby, The deformation of plastically non-homogeneous materials, Philos. Mag. 21 (1970) 399–424.
[81] Y.Z. Tian, S. Gao, L.J. Zhao, S. Lu, R. Pippan, Z.F. Zhang, N. Tsuji, Remarkable transitions of yield behavior and Lüders deformation in pure Cu by changing grain sizes, Scr. Mater. 142 (2018) 88–91.
[82] C.Y. Yu, P.W. Kao, C.P. Chang, Transition of tensile deformation behaviors in ultrafine-grained aluminum, Acta Mater. 53 (2005) 4019–4028.
[83] S. Gao, Y. Bai, R. Zheng, Y. Tian, W. Mao, A. Shibata, N. Tsuji, Mechanism of huge Lüders-type deformation in ultrafine grained austenitic stainless steel, Scr. Mater. 159 (2019) 28–32.
[84] X. Feaugas, H. Haddou, Grain-size effects on tensile behavior of nickel and AISI 316L stainless steel, Metall. Mater. Trans. A. 34 (2003) 2329–2340.
[85] R.Z. Valiev, Superior strength in ultrafine-grained materials produced by SPD processing, Mater. Trans. 55 (2014) 13–18.
[86] S.V. Divinski, G. Reglitz, H. Rösner, Y. Estrin, G. Wilde, Ultra-fast diffusion channels in pure Ni severely deformed by equal-channel angular pressing, Acta Mater. 59 (2011) 1974–1985.
[87] X. Sauvage, G. Wilde, S.V. Divinski, Z. Horita, R.Z. Valiev, Grain boundaries in ultrafine grained materials processed by severe plastic deformation and related phenomena, Mater. Sci. Eng. A. 540 (2012) 1–12.